Electromagnetic multipole of positive and negative parity states in ^{24}Mg by elastic and inelastic electron scattering

Noori S. Manie and Ali A. Alzubadi

Department of Physics, College of Science, University of Baghdad, Baghdad, Iraq

E-mail: noorialsabah74@gamil.com

Abstract

Using shell model and self-consistent Hartree–Fock calculations nuclear structure of ^{24}Mg nucleus has been investigated. In particular, elastic and inelastic electron scattering form factors and transition probabilities are calculated for positive and negative low-lying states. For this purpose, two different shell model spaces have been used. The first one is the *sd* model space for positive parity state and the second one is *sdpf* model space for negative parity states. For all selected excited states, Skyrme interactions are adopted to generate from them a one-body potential in Hartrre-Fock theory to calculate the single-particle matrix elements and compared with those of the harmonic oscillator (HO) and Woods-Saxon (WS) single-particle potentials.

التعددية القطبية الكهرومغناطيسية لحالات التكافؤ االموجبة والسالبة في نواة Mg^{24} عن طريق الاستطارة الإلكترونية المرنة وغير المرنة

نوري صباح مانع وعلي عبد اللطيف كريم

قسم الفيزياء، كلية العلوم، جامعة بغداد، بغداد، العراق

الخلاصة

باستخدام نموذج القشرة وحسابات هارتري فوك المتسقة ذاتيا، تم التحقيق في البنية النووية لنواة Mg^{24}. على وجه الخصوص يتم حساب عوامل التشكل لاستطارة الالكترون المرنة وغير المرنة واحتمالات الانتقال لمستويات التماثل الموجبة والسالبة. تم استخدام نموذجين مختلفين لانموذج فضاء القشرة. الاول *sd* لمستويات التماثل الموجبة والثاني *sdpf* لمستويات التماثل السالبة. لجميع الحالات المثارة المختارة يتم اعتماد تفاعلات سكيرم لتوليد جهد الجسيم المنفرد في نظرية هارتري فوك لحساب عناصر مصفوفة الجسيم المنفرد. قورنت الحسابات مع نتائج دوال الموجة للجسيم المنفرد لجهد المتذبذب التوافقي وجهد وود ساكسون.

Introduction

The study of nuclear structure is usually performed with two major approaches: the first is based on the self-consistent mean-field (SCMF) method [1], which rests on the assumption that in the first approximation, the nucleons can be described as evolving in a mean potential, which emerges from the underlying effective nuclear interaction. The nucleus is thus described as a system of independent nucleons, which are dressed by their averaged interaction with the other particles. The second approach, known as interacting shell model (SM) [2], starts from a given set of single-particle states and directly tackles the correlations between the nucleons in a truncated many-body model space.

The SM allows for configuration mixing (CM) beyond the mean field (MF) [3], so one can take for the MF a

standard phenomenological single-particle model, but then performs a CM calculation involving all many-body states that can be constructed using a more or less broad band of single nucleon states around the Fermi energy [4].

In the present work, we still working by our researches [5] in applying the SM and HF approaches in calculating the inelastic electron scattering form factors for positive and negative parity states in ^{24}Mg nucleus. Johnston and Drake [6] studied the excited-states of ^{24}Mg with excitation energies less than 14.0 MeV using inelastic electron scattering in the momentum transfer range 0.4 to 1.14 fm^{-1}. Zarek et al. [7] measured the electromagnetic form factors for the stronger transitions to negative-parity states in ^{24}Mg for electron energies 90 -280 MeV. Marinelli and Moreira [8] evaluated longitudinal and transverse electron scattering form factors for the 2^+ state at 1.37 MeV of the ^{24}Mg nucleus. The Hartree Fock with different approaches were used for the transverse $E2$ form factor for calculations. The results are discussed and compared with a recent measurement performed for 180˚ electrons scattered from this state. Carvalho and Rowe [9] calculated transverse electron scattering form factors for $0^+ \rightarrow 2^+$ excitations in ^{24}Mg nucleus. In ^{24}Mg, 2^+ state is the first excited, the form factors are computed microscopically. Radhi and Bouchebak [10] discussed inelastic electron scattering to 2^+ and 4^+ states for ^{24}Mg nucleus by taking into account higher energy configurations outside the *sd* shell.

The first one is the *sd*-SM space matrix elements for positive parity states and hence, we present results for new USD-type Hamiltonians called USDE, the USD Hamiltonian [4,11] has provided realistic *sd*-shell wave functions for use in nuclear structure models, and nuclear spectroscopy. The calculations second model space were done in the *sdpf* SM space using the WBP Hamiltonian [12], which is adopted for negative parity states, 1$^-$, 3$^-$ and 5$^-$ for this model, the orbits l$s_{1/2}$, l$p_{3/2}$, and l$p_{1/2}$ are filled (inert ^{16}O nucleus core) and the active (valence) particles were restricted to 1$d_{5/2}$, 1$d_{3/2}$, 2$s_{1/2}$ 1$f_{7/2}$, 1$f_{5/2}$, 2$p_{3/2}$, and 2$p_{1/2}$ orbits with the SDPFMU effective Hamiltonians [12].

The aim of nuclear MF theories is to describe self-bound nuclei in their intrinsic frame where wave-functions are localized. A possible description of a self-bound localized system in terms of Slater determinants could be constructed from single particle wave-functions of a HO or a WS potential. The most suitable framework is that of SCMF [13]. The Skyrme interaction is the most widely used interaction in nuclear structure calculations. The reason is simple: it is a zero-range (but momentum dependent) interaction that greatly simplifies calculations in many-body systems. So, for all excited states, Skyrme interactions are adopted to generate from them a one-body potential in Hartrre-Fock theory to calculate the single-particle matrix elements. The single-particle matrix elements have been calculated with Skyrme-Hartree-Fock (SHF) potential with four different parameterizations in addition to realistic Wood-Saxon (WS) and harmonic oscillator (HO) potentials for comparison. The SHF is a MF potential. One of the main goals of the present calculations is to determine the extent the ability of SM calculations for describing the collective feature, so the obtained form factors from the pure Tassie model transition densities will be compared with results given by the model of Bohr-Mottelson.

Theory and methodology

Electron scattering nuclear form factors for inelastic scattering between an initial (i) and final (f) state or for elastic scattering ($i = f$) are denoted by the longitudinal Coulomb form factor, $F(C\lambda, q, f, i)$ the transverse electric form factor $F(E\lambda, q, f, i)$ and the transverse magnetic form factor $F(M\lambda, q, f, i)$ where λ is the multipolarity [14]. The last two types of form factors can be divided into the components according to the convection currents λc (due to the orbital motion of the nucleons) and the magnetization currents λm (due to the intrinsic magnetic moments of the nucleons), respectively [15].

$$F(E\lambda, q, f, i) = F(E\lambda c, q, f, i) + F(E\lambda m, q, f, i) \tag{1}$$

$$F(M\lambda, q, f, i) = F(M\lambda c, q, f, i) + F(M\lambda m, q, f, i) \tag{2}$$

The final transition form factor expression is given by [16]

$$F(X\lambda x, q, f, i) = (2J_i + 1)^{-1/2} \left[(4\pi)^{1/2} / Z \right] f_{c.m}(q)$$

$$\times \sum_{t_z, x} \frac{g_{fs}(Xx, q, t_z)}{g(Xx, t_z)} \sum_{j, j'} OBTD\ (\lambda, j, j', f, i) o(X\lambda x, q, f, i, t_z) \tag{3}$$

where X stands for C, Mc, Mm, Ec and Em. The factor $(2J_i + 1)^{-1/2}$ arises on going from the reduced matrix element to the matrix element summed over final m substates and averaged over initial m substates. The normalization $\left[(4\pi)^{1/2} / Z \right]$ is chosen to make $F(C0, q = 0$, elastic$) = 1$, as noted above. The term $f_{c.m}$ is the centre of mass form factor that corrects for the lack of translational invariance in shell model wave functions.

$$f_{c.m}(q) = \exp^{(b^2 q^2 / 4A)} \tag{4}$$

where b is the harmonic oscillator length parameter and A is the mass number.

$g_{fs}(Xx, q, t_z)$ are the equivalent q-dependent form factors for free nucleons, $g(Xx, t_z)$ are the free nucleon g factors, given by $g(Mc, t_z) = g(Ec, t_z) = g_l(t_z)$ and $g(Mm, t_z) = g(Em, t_z) = g_s(t_z)$, where g_l and g_s are the free-nucleon g factors, and t_z is proton or neutron isospin.

Multiparticle form factors $O(X\lambda, q, j, j', T_z t_z)$ are given by [17, 18]:

$$O(X\lambda, q, j, j', T_z t_z) = \sum_{j, j'} OBTD\ (\lambda, j, j', f, i, T_z t_z)\ o(X\lambda, q, j, j', t_z) \tag{5}$$

where $o(X\lambda, q, j, j', t_z)$ is single-particle matrix elements and λ is multipolarity, the single particle states $(n\ l\ j)$ are denoted by j. the $OBTD(\lambda, j, j', f, i, T_z t_z)$ in proton-neutron formalism is given by [16]:

$$OBTD\ (\lambda, j, j', f, i, T_z t_z) = \frac{\left\langle f \left\| \left[a^+_{j, t_Z} \otimes \tilde{a}_{j', t_Z} \right]^\lambda \right\| i \right\rangle}{\sqrt{2\lambda + 1}} \tag{6}$$

where T_z, *is* the total nucleus isospin, t_z =1/2 for a neutron and t_z=-1/2 for a proton, while $a_{j,}^+$ and $\tilde{a}_{j'}$ are the creation and destruction operators, respectively.

For central potential, we use Skyrme potential; it is a two-body interaction. One may generate from it a one-body potential in in Hartrre-Fock

theory, as it is done in the codes used. It is supposed to provide the mean field due to all the nucleons which compose the nucleus and approximate the realistic nucleon-nucleon (and nucleon-nucleon-nucleon) forces. Skyrme potential V_{Skyrme} can be written as [19]

$$V_{Skyrme}(\vec{r}_1, \vec{r}_2) = t_0(1 + x_0\hat{P}_\sigma)\delta_{12} + \frac{t_1}{2}(1 + x_1\hat{P}_\sigma)\left[\vec{k}'^2\delta_{12} + \vec{k}^2\delta_{12}\right]$$
$$+ t_2(1 + x_2\hat{P}_\sigma)k'\delta_{12}k + \frac{t_3}{6}(1 + x_3\hat{P}_\sigma)\rho^\alpha(\frac{\vec{r}_1 - \vec{r}_2}{2})\delta_{12} + iW_0\vec{k}'\delta_{12}(\hat{\vec{\sigma}}_1 + \hat{\vec{\sigma}}_2) \times \vec{k}$$
$$+ \frac{t_e}{2}\left(\left[3(\hat{\vec{\sigma}}_1.\vec{k}')(\hat{\vec{\sigma}}_2..\vec{k}') - (\hat{\vec{\sigma}}_1.\hat{\vec{\sigma}}_2)\vec{k}'^2\right] + \delta_{12}\left[3(\hat{\vec{\sigma}}_1.\vec{k})(\hat{\vec{\sigma}}_2.\vec{k}) - (\hat{\vec{\sigma}}_1.\hat{\vec{\sigma}}_2)\vec{k}^2\right]\right)$$
$$+ t_0\left[3(\hat{\vec{\sigma}}_1.\vec{k})\delta_{12}(\hat{\vec{\sigma}}_2.\vec{k}') - (\hat{\vec{\sigma}}_1.\hat{\vec{\sigma}}_2)\vec{k}'\delta_{12}\vec{k}\right] \qquad (7)$$

$$\delta_{12} = \delta(\vec{r}_1 - \vec{r}_2) \qquad (8)$$

$$\hat{K} = \frac{1}{2i}(\vec{\nabla}_1 - \vec{\nabla}_2), \hat{K}' = -\frac{1}{2i}(\vec{\nabla}'_1 - \vec{\nabla}'_2) \qquad (9)$$

which are the relative momentum operators which operate on the wave functions to the right and to the left. $\hat{P}_\sigma$ is the spin-exchange operator given by

$$\hat{P}_\sigma = \frac{1}{2}(1 + \hat{\sigma}_1.\hat{\sigma}_2) \qquad (10)$$

The momentum-dependent terms are introduced to take into account the effect of the finite-range force and are important for the surface properties [20].

The method starts from a SM, and self-consistent Hartree-Fock mean-field calculation with Skyrme interactions. The calculations are

performed with the force SLy4 [21], SkXcsb [22], SkXta [23] and SkXs25 parametrizations [24] which is a suitable representative of the Skyrme forces, in addition to realistic WS, and harmonic oscillator HO [16] potentials for comparison. The single-particle form factors $o(X\lambda, q, j, j', t_z)$ can be reformulated into a concise and uniform notation consisting of integrals over the radial coordinate of spherical Bessel functions $j_\lambda(qr)$ multiplied by single particle transition densities $\rho(r, j, j')$ [25]:

$$o(C\lambda, q, j, j', t_z) = g_l(t_z)e\int \rho(C\lambda, r, j, j', t_z)j_\lambda(qr)d^2r \qquad (11)$$

$$o(M\lambda c, q, j, j', t_z) = g_l(t_z)\mu_N i\int \rho(M\lambda c, r, j, j', t_z)j_\lambda(qr)d^2r \qquad (12)$$

$$o(M\lambda m, q, j, j', t_z) = g_s(t_z)\mu_N i\int \rho(M\lambda m, r, j, j', t_z)j_\lambda(qr)d^2r \qquad (13)$$

$$o(E\lambda c, q, j, j', t_z) = g_l(t_z)\mu_N(1/q)\int \rho(E\lambda c, r, j, j', t_z)j_\lambda(qr)d^2r \qquad (14)$$

$$o(E\lambda m,q,j,j',t_z) = g_s(t_z)\mu_N q \int \rho(E\lambda m,r,j,j',t_z)j_\lambda(qr)d^2r \qquad (15)$$

where $\mu_N = e\hbar/2m_p c = 0.1051 \quad e.fm$ is nuclear magneton with m_p proton mass.

The transition density distribution, can be written as follows [26]:

$$\rho(\lambda,r,j,j') = \rho^{md}(\lambda,r,j,j') + \rho^{core}(\lambda,r,j,j') \qquad (16)$$

According to valence model, the transition density is proportional to the

MS transition density, of the point proton:

$$\rho^{core}(\lambda,r,j,j',t_z)\alpha \quad \rho^{md}(\lambda,r,j,j',t_z) = N \ \rho(\lambda,r,j,j',t_z) \qquad (17)$$

where N is a proportionality constant to be determined in analogy with matrix elements of the gamma-ray transition

operator [27, 25], and are related to the effective charge. The total transition density becomes:

$$\rho(\lambda,r,j,j',t_z) = \quad \rho(\lambda,r,j,j',p) + \rho(\lambda,r,j,j',n)$$
$$= (1+\delta e_p)e\rho(\lambda,r,j,j',p) + \delta e_n e\rho(\lambda,r,j,j',n) \qquad (18)$$
$$\rho(\lambda,r,j,j',t_z) = e_{eff}(p)\rho(\lambda,r,j,j',p) + e_{eff}(n)\rho(\lambda,r,j,j',n) \qquad (19)$$

The quantity δe_p represents the effect of virtual excitation of core protons, and δe_n represents the effect of the of virtual excitation of core protons by

the valance neutrons. The total longitudinal transition density *is* calculated using Tassie [28, 29], and Bohr-Mottelson (B-M) models [29] respectively as*:*

$$\rho^{core}(\lambda,r,j,j',t_z) = N \frac{1}{2}(1+T_z) r^{\lambda-1} \frac{d}{dr}\rho(\lambda,r,j,j',t_z) \qquad (20)$$

$$\rho^{core}(\lambda,r,j,j',t_z) = N \frac{1}{2}(1+T_z) \frac{d}{dr}\rho(\lambda,r,j,j',t_z) \qquad (21)$$

The reduced transition probability is given by [16]:

$$B(X\lambda) = \frac{Z^2}{4\pi} \frac{[(2\lambda+1)!!]^2}{\omega^{2\lambda}}|F(X\lambda,k)|^2 \qquad (22)$$

where $k = E_x/\hbar c$. $B(M1)$ is in units of u_N^2, $B(E2)$ is in units of $e^2 fm^4$, $B(M2)$ is in units of $u_N^2 fm^2$, and $B(E1)$ is in units of $e^2 fm^2$.

Results and discussion

In the present work, using the SM code NuShellX@MSU [30], the

OBDM elements have been calculated. It is a set of wrapper codes written by Alex Brown that use data files for model spaces and Hamiltonians to generate input for NuShellX. NuShellX is a set of computer codes written by Bill Rae [31] that are used to obtain exact energies, eigenvectors and spectroscopic overlaps for low-lying states in shell model Hamiltonian matrix calculations with very large basis dimensions. The OBDM elements are then used to calculate the matrix elements of $C\lambda$, $E\lambda$ and $M\lambda$ operators. As we mentioned

previously. For all electric transitions ($\lambda > 0$), the standard effective charges are used, using the Tassie, and B-M model for CP [26]. For magnetic transitions, free g factors are used. In the present duty calculations is to determine the extent the ability of SM calculations for describing the collective feature, so the obtained form factors from the pure Tassie-model are compared with results the model of B-M. The Coulomb form factors calculated by using CP effects according to valance, Tassie and B-M models, but the transverse form factors calculated by using valance model.

A. Elastic electron scattering form factors of ^{24}Mg nucleus

In the present work, we wish to indicate the possibility of testing SM effective interactions by means of elastic electron scattering calculations. ^{24}Mg nucleus is chosen for this position in the lower of the 2s-1d shell the numbers of active particles outside the ^{16}O core are eight. Extensive elastic electron scattering data are available for this nucleus [32]. *Sd*-SM space calculations were performed for this nucleus using the USDE interactions. Furthermore, the calculations with Skyrme parametrizations are compared with those of the HO and WS single-particle potentials. The oscillator size parameter b=1.82fm chosen to reproduce the measured rms charge radius. The calculated proton, neutron, mass, and charge radii for ^{24}Mg using different single-particle potentials are given in Table 1 along with the experimental data [33]. The concord with the experimental values is seen to be good.

Table 1: Rms radii (fm) for ^{24}Mg nucleus using different single- particle potentials.

Potential	Proton	Neutron	Mass	Charge	Charge Exp.
SLy4	2.950	2.904	2.927	3.032	3.0570 [33]
SkXcsb	2.930	2.893	2.912	3.014	
SKXta	2.978	2.943	2.961	3.060	
SKXs25	2.998	2.948	2.973	3.079	
HO	2.972	2.972	2.972	3.054	
WS	3.028	2.965	2.997	3.109	

The elastic charge C0 form factors of ^{24}Mg are calculated and the results are presented in Fig.1. From this figure, one can see that the theoretical Coulomb factors from the different nuclear single-particle potentials give the calculations of the *sd*-SM space with B-M model present good agreements with the experimental data [32] especially in the range of q from 0.5 up to 2.1 fm^{-1}. However, the result of WS potential coincides with the experimental data better in this range.
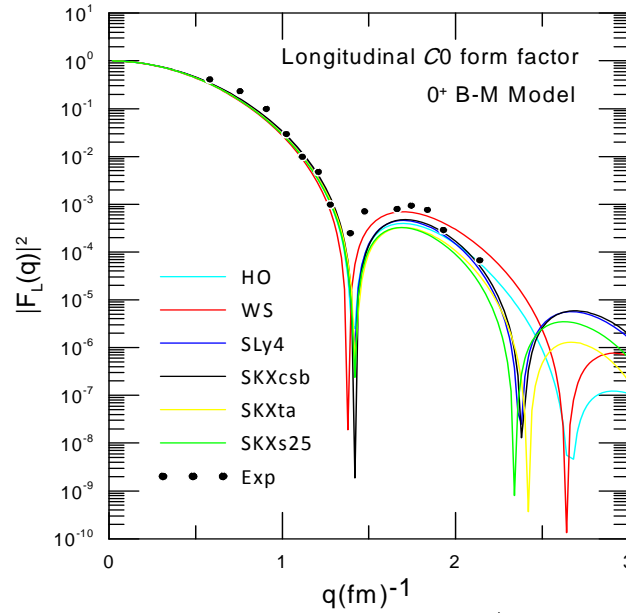
Fig. 1: Theoretical elastic longitudinal form factors for the 0^+, using HO, WS potential and SLy4, SkXcsb, SKXta and SKXs25 parametrizations, compared with the experimental data taken from Ref. [32].

B. The inelastic electron scattering form factors of ^{24}Mg nucleus

1. Positive parity states

Longitudinal electron scattering form factors have been measured for isoscalar transitions to $T = 0$ levels in ^{24}Mg nucleus from the ground-state to the states at 1.37 MeV (2^+), 5.24 MeV (3^+) and 6.01 MeV (4^+) states. Calculated inelastic longitudinal Coulomb $C2$ form factors for the first 2^+ at 1.37 MeV state are displayed in Fig.2 represent the calculation of the result of the various models. For comparison, we also show the SM results obtained in the restricted *sd*-shell single-particle predictions with various nuclear single-particle potentials. The g factor of the first-excited state in the $N = Z$ nucleus ^{24}Mg [33] based on hyperfine fields of hydrogen like Mg ions. By the use of these well-defined hyperfine fields, together with efficient particle and γ-ray detection, the new measurement achieves the accuracy and precision needed to test the predicted departures from g= 0.5 [34]. In general, the calculated longitudinal nuclear coulomb form factor shows a good agreement with the experimental data of the transition from the ground-state to the first excited-state $\lambda =2_1^+$ with 1.37 MeV state for $q>0.3$ fm^{-1}. At low q the results go remarkable well with experimental data [32] except there is an overestimation in the prediction of the position of first diffraction minimum in comparing with experimental data.

33
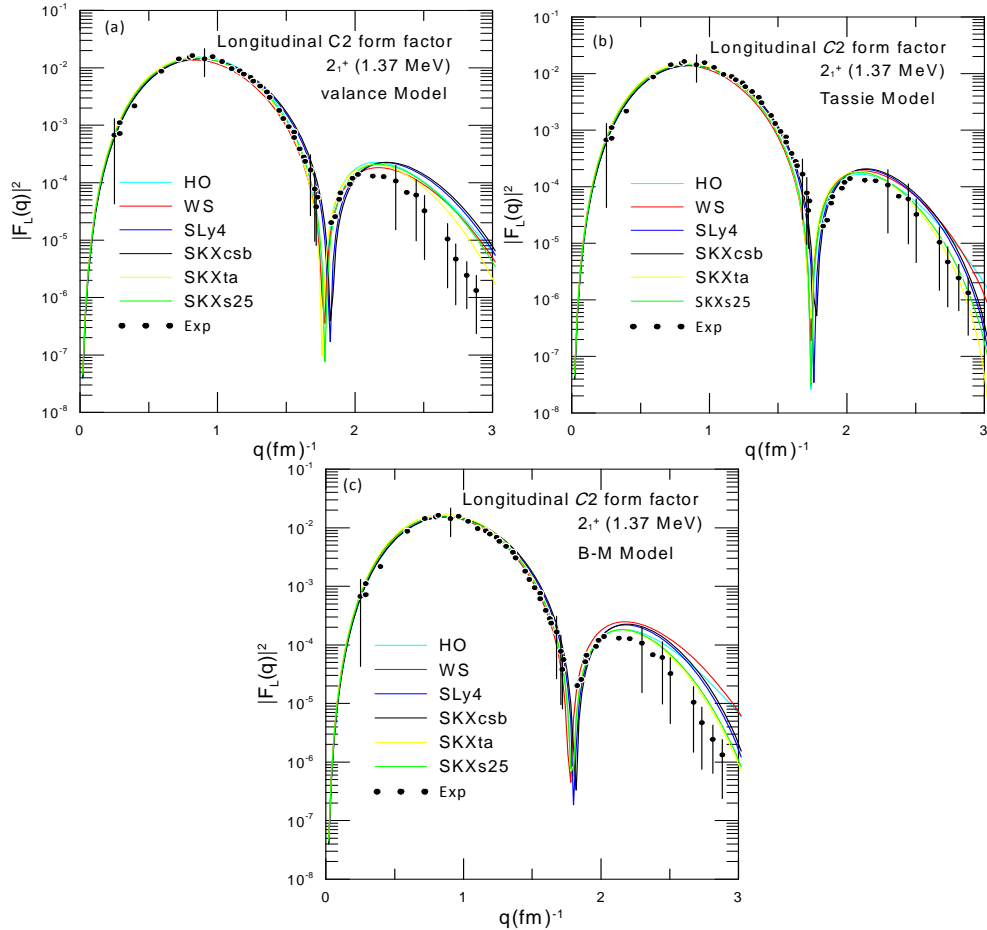
Fig. 2: Theoretical inelastic longitudinal form factors for the first 2$^+$, 1.37 MeV state using different single particle potential compared with the experimental data taken from Ref. [32].

In this work we have undertaken to analyse these results in a framework transverse form factors, the extracted squared transverse $E2$ form factors were described with SM calculation so that effects of different models over the structure of this state were taken into account. This kind of analysis provides unique information about this nucleus. In particular, the first level 2_1^+ at 1.37 MeV was measured at the effective q between 0.87 and 2.07 fm^{-1} are shown in Fig.3, measurements carried out at this level yielded accurate knowledge of form factors up to 3 fm^{-1}, these are single particle calculations has been used. In prevalent, nuclear single-particle potentials resemble each other. For all calculations, the resulting nuclear single-particle potentials lie below the data [27]. However, the calculated transverse form factors for this potentials are found to be in poor concord with the experiments.

In Fig. 4, we also plotted longitudinal $C2$ form factor results for the 2_2^+ at 4.23 state in ^{24}Mg. The available data of this transition are restricted for small region of momentum transfer ($q<1.9$ fm^{-1}). In the first maximum, a best coincidence for the form factors is obtained between the calculation and the experimental data [35].
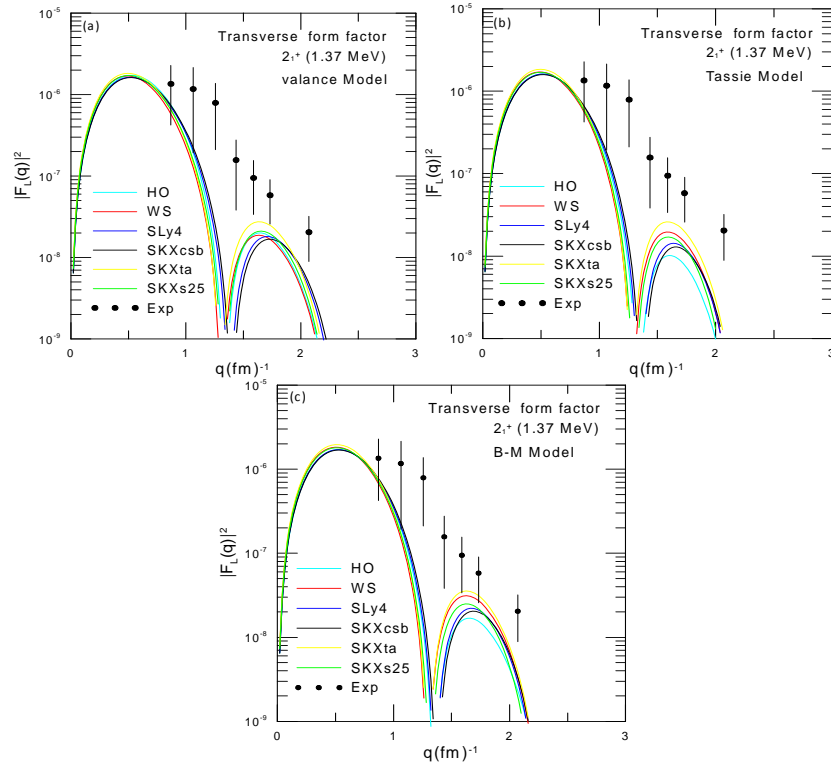
Fig.3: Theoretical transverse form factors for the first 2⁺, 1.37 MeV state using different single particle potential compared with the experimental data taken from Ref. [27].
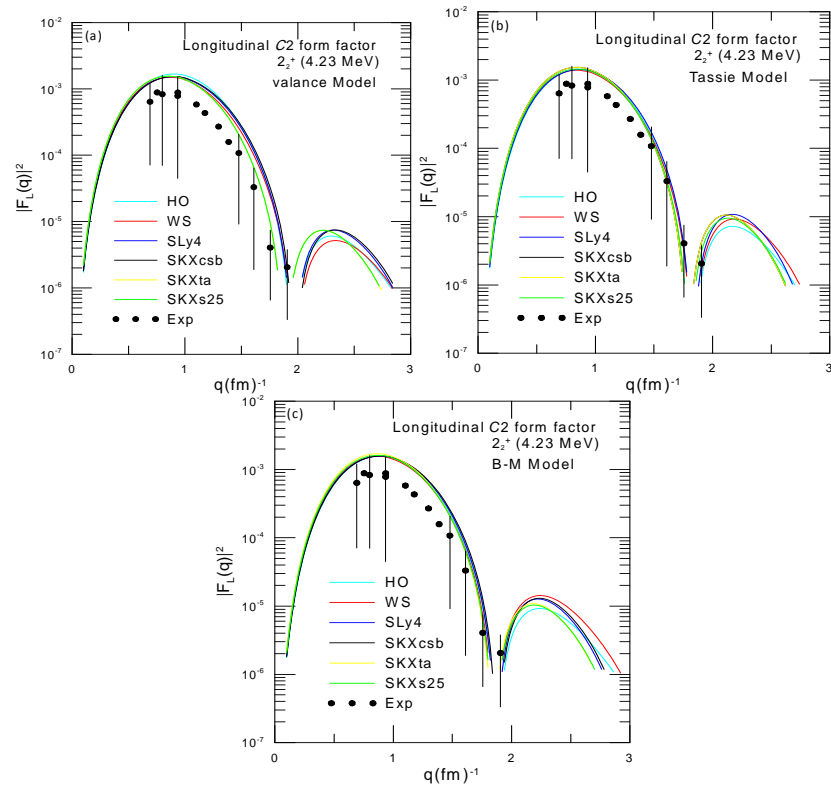
Fig.4: Theoretical longitudinal form factors for the second 2_2^+, 4.23 MeV state using different single particle potential compared with the experimental data taken from Ref. [35].

In Fig.5 the calculated results for inelastic transverse form factors of ^{24}Mg nucleus under study are plotted versus the q and compared with those of experimental results for 3^+ at 5.24 MeV state the total contribution is represented using different single particle potentials and obtained by taking valance model assuming a $M3$ transition and the best fit obtained is shown with the data in this Figure. The experimental data, shown by circles, are taken from Ref. [36].

The inelastic longitudinal $C4$ form

factors for the states 4.12 MeV and 6.01 MeV in ^{24}Mg are displayed in Figs. 6 and 7. It can be seen that the calculated results using different models are a satisfactory with the experimental data for the region of momentum transfer $q \leq 3$ fm^{-1}, the obtained results for the longitudinal $C4$ form factors become in a good agreement with the experimental data [7, 32] throughout the whole range of q and from these figures, one can see that the coulomb form factors calculated are very close to each other.
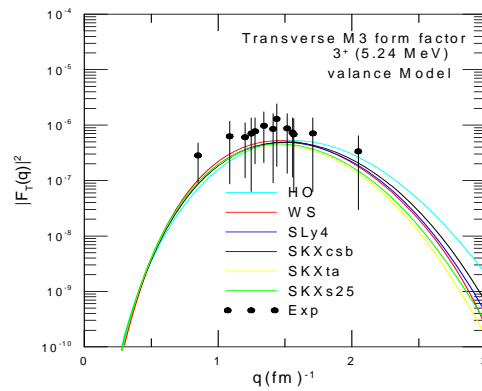
Fig.5: Theoretical transverse form factors for the first 3^+, 5.24 MeV state using different single particle potential compared with the experimental data taken from Ref. [36].
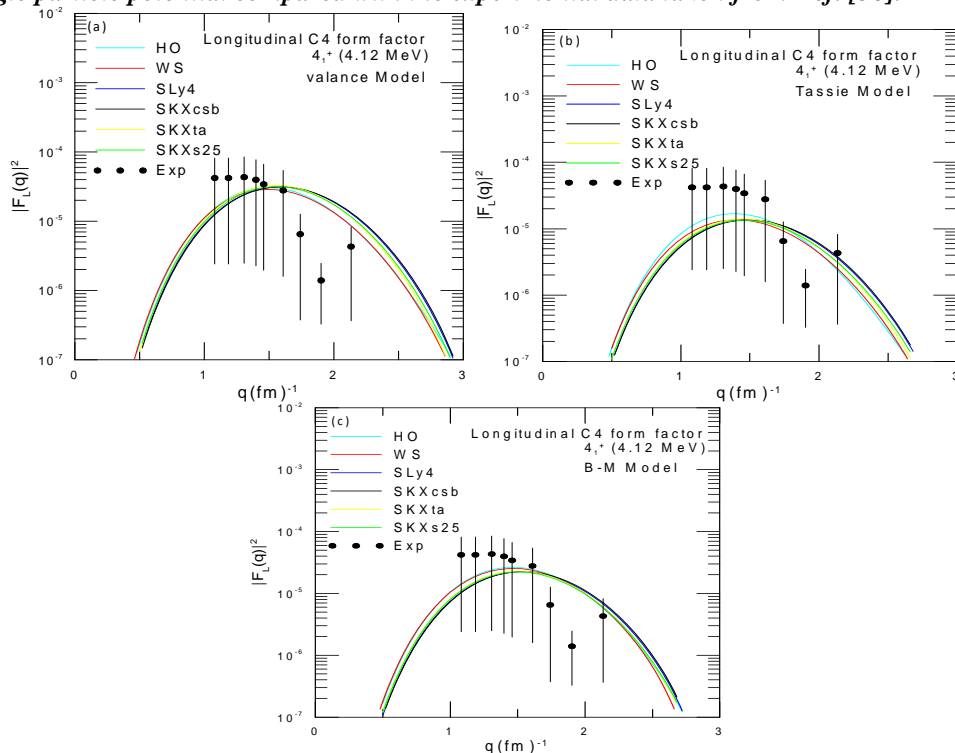
Fig.6: Theoretical longitudinal form factors for the first 4^+, 4.12 MeV state using different single particle potential compared with the experimental data taken from Ref. [33].
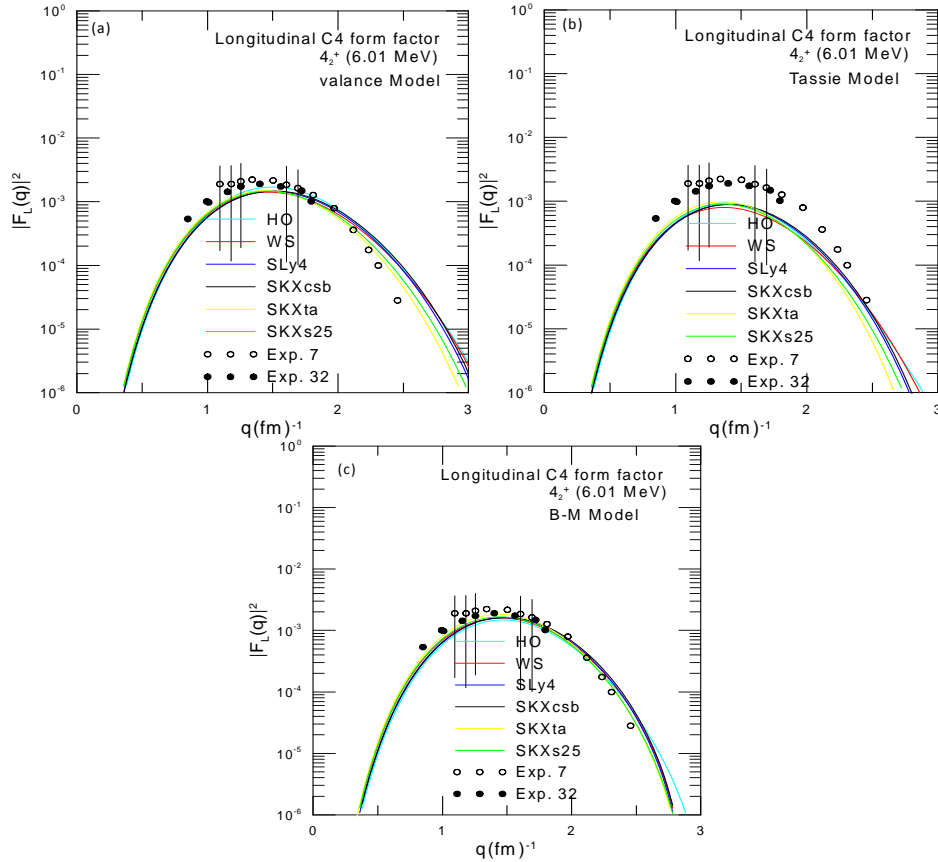
Fig.7: *Theoretical longitudinal form factors for the second 4⁺, 6.01 MeV state using different single particle potential compared with the experimental data taken from Ref. [7, 27].*

2. Negative parity states

In this work we have presented the results of high resolution form factor measurements for 1^-, 3^- and 5^- states, in ^{24}Mg. 1^- $T= 0$ state have been identified at excitation energies of 7.553 MeV. The *sdpf* SM space with *SDPFMU* two-body effective interaction [38] are used in reproducing the total squared form factor the data for all q values, as shown by various nuclear single-particle potentials. In Fig. 8, the total squared form factors for the lowest 1^- $T= 0$ state at excitation energy of 7.553 MeV are compared with the experimental data of Ref. [6]. It can be seen that the results inclusion by adopting the various models enhances the calculations and describes the data very well at both second and third

maxima and locate the diffraction minimum at its right position.

3^- $T= 0$ state have been identified at excitation energies of 7.616 MeV. In Fig. 9, the total squared form factors for the lowest first 3^- $T= 0$ state at excitation energy of 7.616 MeV are compared with the experimental data of Ref. [6]. In general, the results lie agreement with the experimental data.

In Fig. 10, the total squared form factors for the 5^- $T= 0$ state at excitation energy of 10.030 MeV, are compared with the experimental data of Ref. [6]. The multipolarity included in this transition is pure longitudinal *sdpf* SM space predictions of the longitudinal $C5$ with *SDPFMU* effective interaction. All results in this state are close to each other and slightly under predict the experimental data.
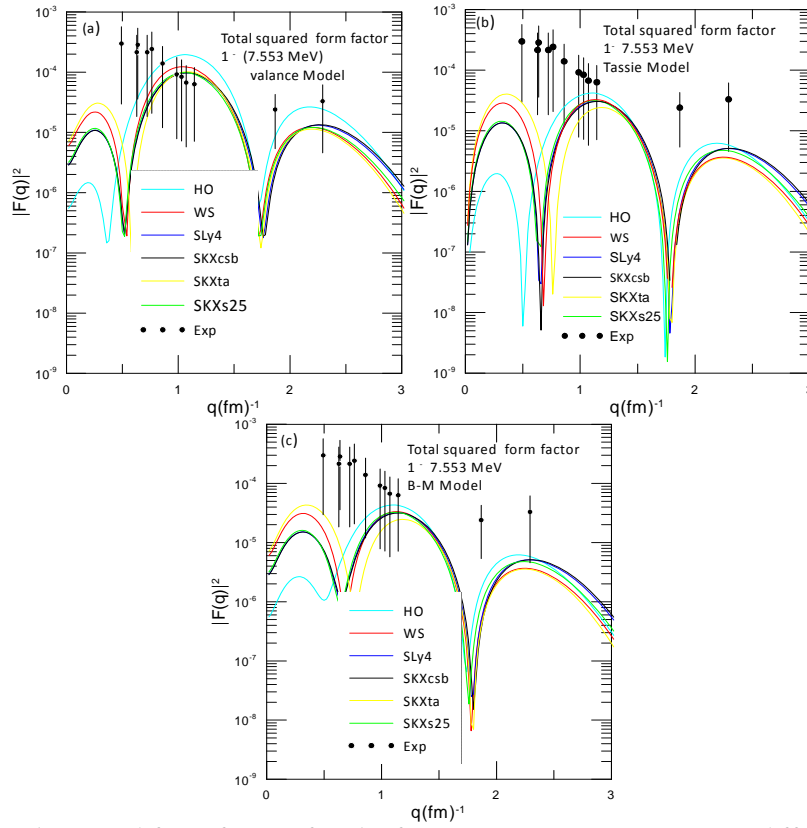
Fig. 8: Total squared form factors for the first 1^-, 7.553 MeV state using different single particle potential compared with the experimental data taken from Ref. [6].
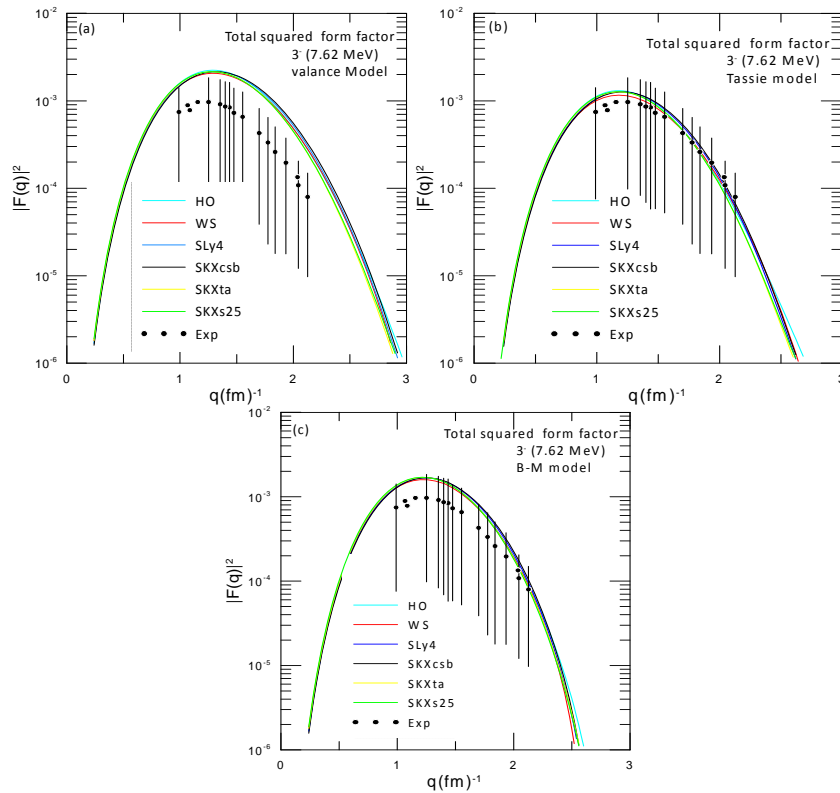
Fig. 9: Total squared form factors for the second 3_1^-, 7.62 MeV state using different single particle potential compared with the experimental data taken from Ref. [6].
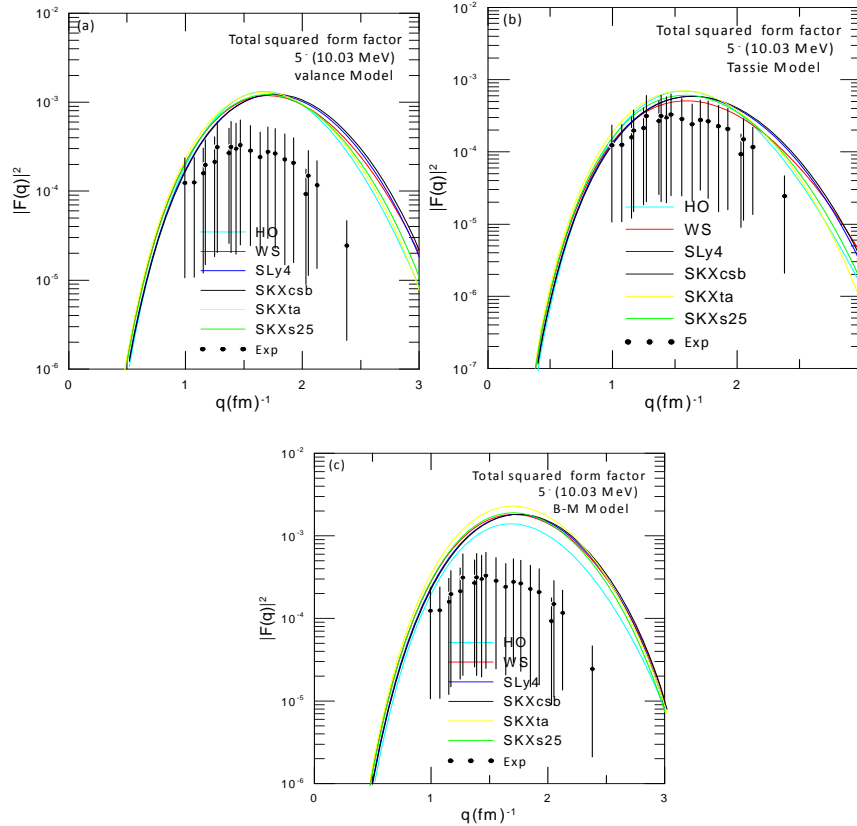
Fig. 10: Total squared form factors for the second 5⁻, 10.03 MeV using different single particle potential compared with the experimental data taken from Ref. [6].

C. Reduced transition probabilities

The reduced transition probabilities $B(C2\uparrow)$ and $B(C4\uparrow)$ are also calculated for the positive-parity states *sd*-shell nuclei and compared with the available experimental data. Also, an excellent overlap between the experimental [39, 40] and calculated $B(C2\uparrow)$. An exception is the $B(C4\uparrow)$ value. These values are displayed in Table 2. The theoretical $B(C1\uparrow)$, $B(C3\uparrow)$ and $B(C5\uparrow)$ values, are calculated for the negative-parity states *sdpf* SM spaces and the experimental $B(C3\uparrow)$ values, are listed in Table 3. The observables such as $B(C1\uparrow)$, $B(C2\uparrow)$ and $B(C3\uparrow)$, within the low-lying state, provide important information about the nuclear structure [41, 42].

Table 2: Comparison of experimental transition probabilities with predictions of Present Work for positive-parity states in ^{24}Mg.

E (MeV)	J^π	Present Work $B(C2\uparrow)(e^2 \text{ fm}^4)$	Experiment	Present Work $B(C4\uparrow)(e^2 \text{ fm}^8)$	Experiment
1.37	2_1^+	427.5	428±9 [39]		
1.37	2_2^+	45.50	22±2 [40]		
6.01	4^+			682	43 ± 6 [43]

Table 3: Comparison of experimental transition probabilities with predictions of Present Work for negative- parity states in ^{24}Mg.

E (MeV)	$\mathcal{J}^{\pi}$	Present Work $B(C1\uparrow)(e^2\text{fm}^2)$	Present Work $B(C3\uparrow)(e^2\text{ fm}^6)$	Present Work $B(C5\uparrow)(e^2\text{ fm}^{10})$	Experiment [44]
7.553	1_1^-	0.721×10^{-10}			
8.438	1_2^-	0.0			
9.148	1_3^-	0.8982×10^{-10}			
7.616	3_1^-		0.121×10^4		5.62×10^2
8.358	3_2^-		0.148×10^2		1.58×10^2
10.03	5^-			0.1406×10^7	
13.86	5^-			0.1406×10^7	

IV. Conclusions

Now, we are still continuing our researches in applying the SHF with SM results to study the nuclear structure of ^{24}Mg nucleus containing both positive and negative parity states. Especially, the inelastic electroexcitation form factors in the momentum-transfer range $0.0 < q < 3.0$ fm^{-1}, and transition probabilities have been calculated. Four single particle potentials, we have considered the Skyrme parameterizations, HO and WS potentials. In every potential parameterization exist which provide a fine description of nuclear bulk properties and also of excited states of nuclei. From the outcomes of our calculations, it is possible to conclude that the reproduced charge rms, form factors and transition probabilities using the *sd* and *sdpf* SM spaces with different parameterizations are broadly consistent with the major trends of the available experimental data without any additional fit of parameters. We can certain that combining these two methods can accommodate very well in the elastic and inelastic nuclear properties and work better for low lying states than for higher excitations. In addition, it can be used for reproducing the positive and negative parity states after choosing the suitable model space, effective two-body interaction and parameterization to get highly descriptive and predictive results when investigating different nuclear configurations as well as for unstable nuclei.

References

[1] C. Robin, N. Pillet, D. Peña Arteaga, J.-F. Berger, Phys. Rev., C 93 (2016) 024302.

[2] P. Ring and P. Schuck "The Nuclear Many-Body Problem" Springer-Verlag, New York (1980).

[3] B. A. Brown, Prog. Part. Nucl. Phys, 47 (2001) 517-599.

[4] B. A. Brown and B. H. Wildenthal, Annu. Rev. Nucl. Part. Sci. 38 (1988) 29-66.

[5] R.A. Radhi, A. A. Alzubadi, E. M. Rashed, Nucl. Phys. A 947 (2016) 12-25.

[6] A Johnston, and T E Drake, J. Phys. A. Math., Nucl. Gen. 7 (1974) 898-935.

[7] H. Zarek, S. Yen, B.0. Pich, and T. E. Drake, C. F. Williamson, S. Kowalski, C. P. Sargent. Phys. Rev. C 29 (1984) 5.

[8] Jose Ricardo Marinelli and Jose Roberto Moreira, Phys Rev, C 39, 1242 (1989) 4.

[9] M. J. Carvalho and D. J. Rowe, Nucl Phys, A 618 (1997) 65-86.

[10] R.A. Radhi and A. Bouchebak, Nucl Phys, A 716 (2003) 87-99.

[11] B. H. Wildenthal, Prog. Part. Nucl. Phys., 11 (1984) 5-51.

[12] E. K. Warburton and B. A. Brown, Phys. Rev., C 46, 3 (1992) 923-944.

[13] J. Stone and P. G. Reinhard, Prog. Part. Nucl. Phys., 58 (2007) 587- 657.

[14] R. A. Radhi, Euro. Phys. J., A 34 (2007) 107-111.

[15] T. M. Shneidman, R. V. Jolos, R. Krucuken, A. Aprahamian, D. Cline, J. R. Cooper, M. Cromaz, R. M. Clark, C. Hutter, A.O. Macchiavelli, W. Scheid, M.A. Stoyer, C.Y. Wu, Eur. Phys. J., A 25 (2005) 387- 396.

[16] B. A. Brown, Lecture Notes in Nuclear Structure Physics. National Superconducting Cyclotron Laboratory, Michigan State University and Department of Physics and Astronomy (2005).

[17] P.J. Brussaard and P.W Glaudemans "Shell model applications in nuclear spectroscopy" North-Holland, Amsterdam (1977).

[18] J. W. Negele, D. Vautherin, Phys. Rev., C 5 (1972) 1472.

[19] D. Vautherin and D. M. Brink, Phys. Rev. C 5 (1972) 231.

[20] H. Sagawa, B. A. Brown, O. Scholten, Phys. Lett., 159B (1985) 228- 232.

[21] E. Chabanat, R. Bonche, R. Haensel, J. Meyer, R. Schaeffer, Nucl. Phys., A 635 (1998) 231- 256.

[22] B. A. Brown, W. A. Richter, R. Lindsay, Phys. Lett., B 483 (2000) 49-54.

[23] B. A. Brown, T. Duguet, T. Otsuka, D. Abe, T. Suzuki, Phys. Rev., C 74 (2006) 061303.

[24] B. A. Brown, G. Shen, G. C. Hillhouse, J. Meng, A. Trzcinska, Phys. Rev., C 76 (2007) 034305.

[25] B. A. Brown, B. H. Wildenthal, C.F. Williamson, F. N. Rad, S. Kowalski, Hall Crannell, J. T. O'Brien, Phys. Rev., C 32, 4 (1985) 1127- 1156.

[26] Xiangdong.Ji and B.H. Wildenthal, Phys. Rev., C 38 (1988) 2849.

[27] B. A. Brown, R. Radhi, B.H. Wildenthal, Phys. Rep., 101 (1983) 313-358.

[28] H. Ui and T. Tsukamoto, Prog. Theor. Phys., 51 (1974) 1377-1386.

[29] A. Bohr and B. R. Mottelson, "Nuclear Structure Vol II", World Scientific (1998).

[30] B. A. Brown and W. D. M. Rae, Nucl. Data. Sheet, 120 (2014) 115-118.

[31] NuShellX, W.D.M. Rae, http://www.garsington. eclipse.co.uk.

[32] I. Angeli, K.P. Marinova, Atomic Data and Nuclear Data Tables, 99, 1 (2013) 69-95.

[33] S. Raman, C. W. Nestor, Jr., P. Tikkanen, Atomic data and Nuclear Data Tables, 78 (2001) 1-128.

[34] A. Kusoglu, A. E. Stuchbery, G. Georgiev, B. A. Brown, A. Goasduff, L. Atanasova, D. L. Balabanski, M. Bostan, M. Danchev, P. Detistov, K. A. Gladnishki, J. Ljungvall, I. Matea, D. Radeck, C. Sotty, I. Stefan, D. Verney, D. T. Yordanov, Phys. Rev. Letters, PRL 114 (2015) 062501.

[35] A. Hotta, R. S. Hicks, R. L. Huffman, G. A. Peterson, R. J. Peterson, J. R. Shepard, Phys. Rev., C 36 6 (1987) 2212-2220.

[36] I. J. D. MacGregor, A. Johnston, J. S. Ewing, Nucl. Phys., A 412, 1 (1984) 1-12.

[37] H. Zarek, S. Yen, B. O. Pich, T. E. Drake, C. F. Williamson, S. Kowalski, C. P. Sargent, W. Chung, B. H. Wildenthal, M. Harvey, H. C. Lee, Phys. Letters.. B 80, 1-2 (1978) 26-29.

[38] Yutaka Utsuno, Takaharu Otsuka, B. Alex Brown, Michio Honma, Takahiro Mizusaki, Noritaka Shimizu, Phys. Rev., C 86 (2012) 051301.

[39] R. M. Lombard and G. R. Bishop, Nucl. Phys., A 101, 3 (1967) 601- 624.

[40] R. S. Hicks, A. Hotta, J. B. Flanz, H. deVries, Phys. Rev., C 21 (1980) 6.

[41] F. Iachello, P. Van Isacker "The Interacting Boson-Fermion Model" Cambridge University Press (1991).

[42] A. Jalili Majarshin, M.A. Jafarizadeh, Nucl. Phys., A 968 (2017) 287- 325.

[43] R. A. Radhi, A. K. Hamoudi, K.S. Jassim, Indian J. Phys., 81 (2007) 683-695.

[44] B. H. Wildenthal and J. B. McGrory, Phys. Rev., C 7 (1973)1143.